



RESEARCH ARTICLE

10.1002/2015JC011010

Estimating diffusivity from the mixed layer heat and salt balances in the North Pacific

Meghan F. Cronin¹, Noel A. Pelland², Steven R. Emerson², and William R. Crawford³¹NOAA Pacific Marine Environmental Laboratory, Seattle, Washington, USA, ²School of Oceanography, University of Washington, Seattle, Washington, USA, ³Institute of Ocean Science, Fisheries and Oceans Canada, Sidney, Canada

Key Points:

- Diffusivity, corresponding to the diffusive flux at the base of mixed layer, is estimated
- This diffusivity has a seasonal cycle, with lower values during summer
- Diffusivity values in the Kuroshio Extension Observatory region are larger than at Station Papa

Correspondence to:

M. F. Cronin,
Meghan.F.Cronin@noaa.gov

Citation:

Cronin, M. F., N. A. Pelland, S. R. Emerson, and W. R. Crawford (2015), Estimating diffusivity from the mixed layer heat and salt balances in the North Pacific, *J. Geophys. Res. Oceans*, 120, 7346–7362, doi:10.1002/2015JC011010.

Received 29 MAY 2015

Accepted 28 SEP 2015

Accepted article online 1 OCT 2015

Published online 11 NOV 2015

Abstract Data from two National Oceanographic and Atmospheric Administration (NOAA) surface moorings in the North Pacific, in combination with data from satellite, Argo floats and glider (when available), are used to evaluate the residual diffusive flux of heat across the base of the mixed layer from the surface mixed layer heat budget. The diffusion coefficient (i.e., diffusivity) is then computed by dividing the diffusive flux by the temperature gradient in the 20 m transition layer just below the base of the mixed layer. At Station Papa in the NE Pacific subpolar gyre, this diffusivity is 1×10^{-4} m²/s during summer, increasing to $\sim 3 \times 10^{-4}$ m²/s during fall. During late winter and early spring, diffusivity has large errors. At other times, diffusivity computed from the mixed layer salt budget at Papa correlate with those from the heat budget, giving confidence that the results are robust for all seasons except late winter-early spring and can be used for other tracers. In comparison, at the Kuroshio Extension Observatory (KEO) in the NW Pacific subtropical recirculation gyre, somewhat larger diffusivities are found based upon the mixed layer heat budget: $\sim 3 \times 10^{-4}$ m²/s during the warm season and more than an order of magnitude larger during the winter, although again, wintertime errors are large. These larger values at KEO appear to be due to the increased turbulence associated with the summertime typhoons, and weaker wintertime stratification.

1. Introduction

Wind mixing, surface heat loss to the atmosphere, wave-generated mixing, shears associated with near-inertial oscillations, and other processes cause turbulence values in the surface “mixed layer” to be several decades larger than found deeper in the interior thermocline [Fernández-Castro *et al.*, 2014]. Diffusive transport through the stratified water column below the base of the mixed layer is typically expressed as a downgradient flux that is proportional to the property gradient, with the proportionality factor referred to as the “diffusion coefficient” or “eddy diffusivity,” hereinafter referred to simply as “diffusivity.” Because our observations generally have 20 m vertical spacing, we assume that the diffusive flux across the mixed layer base is equivalent to the downgradient flux at the center of a 20 m layer directly below the base of the mixed layer. Turbulence in this transition layer can still be relatively strong so that even weak vertical gradients in the physical or biogeochemical tracers can result in large diffusive fluxes. Consequently, diffusive mixing tends to be a leading-order process governing the surface layer properties [Lee *et al.*, 2015]. Understanding the magnitude and variability of the diffusion coefficient is thus critical for studies of the exchange of heat, freshwater, and biogeochemical tracers between the surface layer of the ocean and the main pycnocline.

Diffusive transport is traditionally estimated from shipboard observations of the temperature or velocity microstructure [e.g., Schmitt *et al.*, 1988; Polzin *et al.*, 1997] or through passive tracer release experiments [e.g., Ledwell *et al.*, 2011]. Such measurements, however, are labor intensive and have sparse spatial and temporal coverage that does not in general resolve seasonal cycles. In this analysis, we use a combination of autonomous data from surface moorings, satellites, Argo floats, and a glider to estimate the seasonal cycle of the diffusive flux at the base of the mixed layer and its corresponding diffusivity from the residual of the mixed layer heat and salt budgets. With the diffusivity estimates presented here, the diffusive flux of heat, salt, and other properties can potentially be estimated simply using information about the property's vertical profile (e.g., A. J. Fassbender, C. L. Sabine, and M. F. Cronin, Net community production and calcification from seven years of NOAA Station Papa Mooring measurements, submitted to *Global Biogeochemical Cycles*, 2015).

© 2015. The Authors.

This is an open access article under the terms of the Creative Commons Attribution-NonCommercial-NoDerivs License, which permits use and distribution in any medium, provided the original work is properly cited, the use is non-commercial and no modifications or adaptations are made.

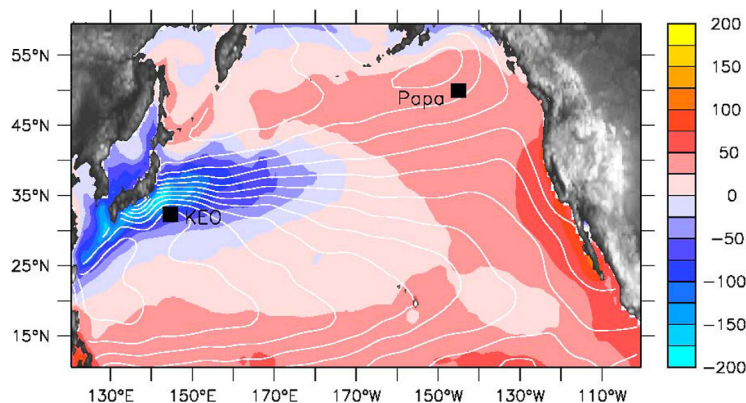


Figure 1. Mean climatological net surface heat flux [Yu and Weller, 2007] in the North Pacific in units W/m^2 . The KEO and Papa stations are indicated by a black square. A positive net surface heat flux indicates heat loss by ocean to the atmosphere. White contours indicate mean absolute sea level [Niiler et al., 2003].

Two National Oceanographic and Atmospheric Administration (NOAA) surface moorings are used, located at Station Papa (50°N , 145°W) in the northeast Pacific Subarctic gyre, and the Kuroshio Extension Observatory (KEO; 32.3°N , 144.5°E) in the northwest Pacific subtropical recirculation gyre (Figure 1). The KEO region is fundamentally different than Station Papa and thus comparisons of results between these two locations of contrasting oceanography and surface fluxes may provide information about the processes affecting diffusivity. KEO, for example, is in a region of mean net surface heat loss, while Station Papa is in a region of mean heat gain. At KEO the top of the main pycnocline and wintertime mixed layer are hundreds of meters deep, while at Station Papa the main pycnocline is shallow and reinforced by a shallow halocline so that the wintertime mixed layer is no more than roughly 100 m deep. While both locations are in the North Pacific storm track and experience large winter storms, KEO also experiences frequent warm season typhoons [Tomita et al., 2010]. Currents and horizontal gradients are weak at Station Papa, but can be very large at KEO. We note that it appeared that errors were large when advection was large at KEO; diffusivity was only computed during periods when advection and the errors were minimal. The KEO diffusivity values should be considered representative of the recirculation gyre south of the Kuroshio Extension (KE), not of the KE itself. At both sites, the time series extends from 4 to 5 years so that a seasonal climatology can be computed.

This study complements Cronin et al.'s [2013] mixed layer temperature budget analysis of the erosion and formation of the seasonal thermocline in the Kuroshio Extension recirculation gyre. In the present study, a seasonal cycle of the diffusivity at the base of the mixed layer is calculated from the mixed layer *heat* budget rather than from the mixed layer *temperature* budget. It is shown here that this provides a more direct relation to the diffusive flux. As with Cronin et al. [2013], satellite-based sea surface temperature (SST) fields are used to estimate the effects of heat advection. In addition, at Station Papa where advection is generally weak, mixed layer salinity gradients could be estimated from glider butterfly patterns and Argo floats. Thus, at Station Papa both the heat and salt mixed layer budgets are evaluated and used to obtain independent estimates of the diffusivity. In the absence of errors and processes such as salt fingers, we would expect that these values of diffusivity should be nearly the same. A reasonable agreement thus helps provide confidence that these diffusivity estimates can be used for other budgets, e.g., for carbon (Fassbender et al., submitted manuscript, 2015) or oxygen [Emerson and Stump, 2010]. As will be discussed, the diffusivity values at the base of the mixed layer have a seasonal cycle, have geographic variations, and are significantly larger than the values found in the thermocline and interior of the ocean.

2. Methodology and Data

Following Cronin et al. [2013] and Stevenson and Niiler [1983], the mixed layer heat budget can be expressed as:

$$\rho_0 C_p h \frac{\partial T}{\partial t} = \underbrace{Q_0 - Q_{pen}|_{z=-h}}_1 - \underbrace{\rho_0 C_p h \mathbf{u} \cdot \nabla T}_2 - \underbrace{\rho_0 C_p \left(w_{-h} + \frac{dh}{dt} \right) (T - T_{-h})}_3 - \underbrace{\rho_0 C_p \overline{wT}}_{z=-h}}_4 \quad (1)$$

where T and \mathbf{u} are the vertically averaged temperature and horizontal velocity within the mixed layer, Q_0 is the net flux of heat into the ocean surface and Q_{pen} is the radiative heat flux penetrating through the base of the mixed layer (h), $\rho_0 C_p$ is the volumetric heat capacity of seawater (taken to be $4.088 \times 10^6 \text{ J } ^\circ\text{C}^{-1} \text{ m}^{-3}$), w_{-h} is the vertical velocity at the base of the mixed layer and is positive for upward flow, T_{-h} is the temperature at the base of the mixed layer, and term 4 represents the upward diffusive heat flux through the base of the mixed layer to be diagnosed. As in Cronin *et al.* [2013], horizontal diffusion and sheared-stratified flow convergence of heat within the mixed layer are assumed to be small and are neglected. We expect that these are much better assumptions at Station P than at KEO, where horizontal gradients can at times be large.

Term 3 on the right-hand side (RHS) of (1) includes both cooling due to large-scale entrainment mixing (a turbulent process) and warming due to detrainment when the mixed layer depth shoals rapidly due to restratification. If the mixed layer were perfectly isothermal, detrainment would not contribute to a change in T during shoaling, and thus detrainment could be set to zero during these periods. However, in a practical sense, when the mixed layer is defined to be the depth range over which a very small (but nonzero) increment in stratification occurs, the "mixed layer" must have some weak stratification. Thus, a shoaling mixed layer may indeed contribute to a change in T , and we retain the detrainment term for accuracy. While large-scale entrainment mixing causes the mixed layer to deepen and cool over the course of several days without affecting the temperature below the mixed layer, diffusive mixing (term 4 on RHS of (1)) causes a transport of heat from the mixed layer to the waters below. Diffusive mixing thus can cause cooling within the mixed layer and warming below, thus reducing the stratification of the upper ocean (e.g., at Station Papa: Large *et al.*, [1986]; Large and Crawford, [1995]; Dohan and Davis, [2011]).

Likewise the mixed layer salt budget can be expressed as:

$$h \frac{\partial S}{\partial t} = (E - P)S_0 - h\mathbf{u} \cdot \nabla S - \left(w_{-h} + \frac{dh}{dt} \right) (S - S_{-h}) + \overline{w'S'} \Big|_{z=-h} \tag{2}$$

where S is the vertically averaged salinity within the mixed layer, E and P are the surface evaporation and precipitation, respectively, and S_0 and S_{-h} are the salinities at the air-sea interface and the base of the mixed layer, respectively. As will be discussed further, the heat and salt fluxes at the base of the mixed layer can be estimated for extended periods of time as the residual of (1) and (2). These we relate to diffusivity coefficients κ_T and κ_S according to:

$$\overline{w'T'} \Big|_{z=-h} = -\kappa_T \frac{\partial T}{\partial z} \Big|_{z=-h} \tag{3a}$$

$$\overline{w'S'} \Big|_{z=-h} = -\kappa_S \frac{\partial S}{\partial z} \Big|_{z=-h} \tag{3b}$$

where the temperature and salinity stratifications are computed from values at the base of mixed layer and 20 m below the mixed layer depth. Assuming that heat and salt diffusivities are equivalent to a mass diffusivity, these coefficients should be equivalent and can be used to estimate the diffusion of other properties such as carbon. Equations (1) and (2) thus provide independent methods for estimating diffusivity; agreement of diffusivity estimated from these two methods provides a useful validation test that the estimates are realistic.

The primary data used to evaluate (1) and (2) are daily averaged time series from the NOAA Station Papa surface mooring at 50.1°N, 144.9°W and the NOAA KEO surface mooring at 32.3°N, 144.6°E (Figure 1). The KEO mooring has been described by Cronin *et al.* [2013] and so here we focus on details of the Station Papa mooring. Unlike the KEO mooring whose line length to water depth scope is 1.4, Papa was a taut line mooring with scope < 1. Its watch circle radius is only 1.4 km and the location of the buoy never varied from the nominal site by more than 8 km throughout the entire 6 year study period. The Papa mooring was first deployed in mid-June 2007 as part of a carbon cycle process study [Emerson *et al.*, 2011] but has continued as an ongoing OceanSITES time series reference station [Send *et al.*, 2010]. The Station Papa study period thus extends from mid-June 2007 to June 2013. The KEO study period is June 2004 through June 2014. Due to data gaps, the number of realizations of a given month is quite a bit less than 6 and 10 years for Papa and KEO time series, respectively, particularly for winter and spring months.

Papa Daily Data

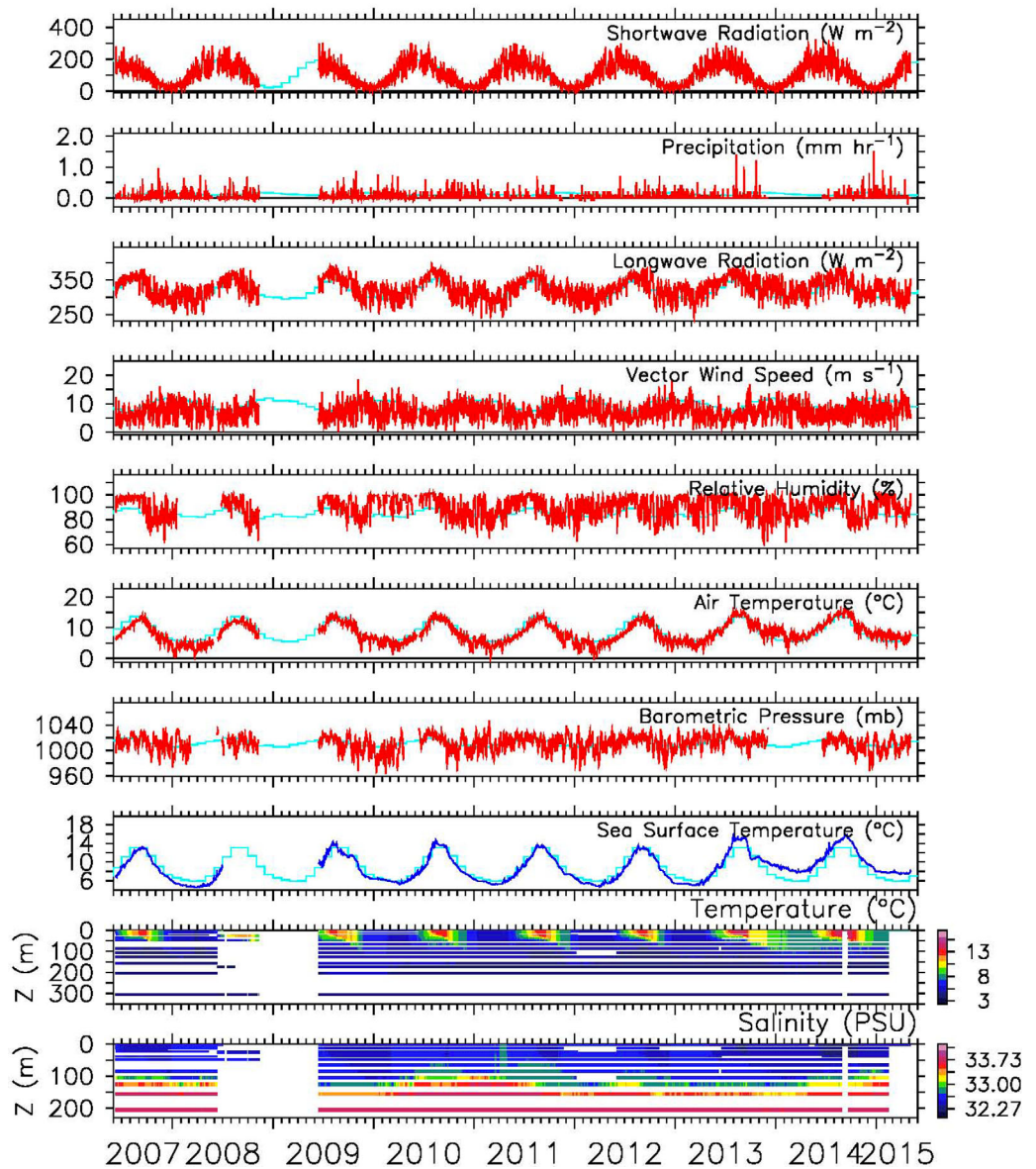


Figure 2. Daily averaged surface data as measured by the NOAA Station Papa mooring. The light blue lines show the monthly climatologies.

Mooring surface measurements include: wind speed and direction (from a sonic anemometer), air temperature and relative humidity, barometric pressure, rain rate, solar and long-wave radiation, and SST and salinity at 1.2 m depth (Figure 2). Their sampling strategies are described in *Cronin et al.* [2013] and errors are described in *Kubota et al.* [2008]. These data are used to compute both the turbulent and radiative components of the net surface heat flux, Q_0 :

$$Q_0 = Q_{sw} - Q_{lw} - Q_{lat} - Q_{sen} \tag{4}$$

where the net solar radiation (Q_{sw}) and net longwave radiation (Q_{lw}) are estimated using the measured downwelling shortwave and longwave radiations. A climatological seasonal cycle for albedo is used based upon International Satellite Cloud Climatology Project (ISCCP) data. Likewise, latent (Q_{lat}) and sensible (Q_{sen}) heat fluxes are computed using the COARE v3.0 bulk algorithm [Fairall et al., 2003] with hourly averaged data and include both the warm layer and coolskin corrections. The amount of solar radiation that

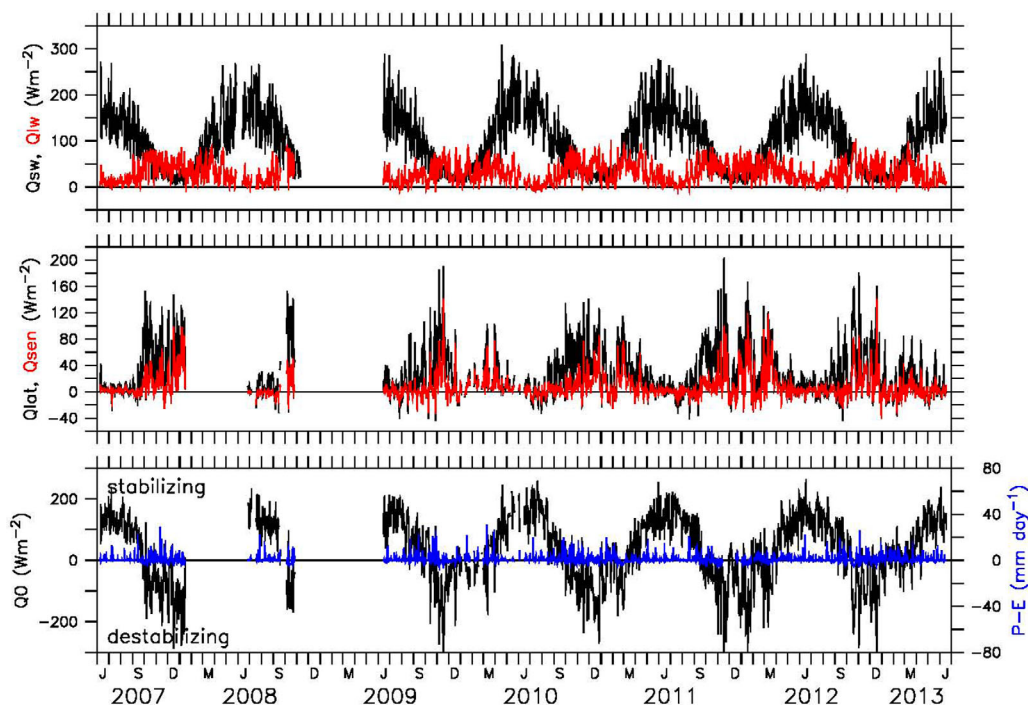


Figure 3. Daily averaged air-sea heat fluxes estimated from hourly Station Papa data. (top) Net solar (black) and net longwave (red) radiations; (middle) latent (black) and sensible (red) heat loss; and (bottom) daily averaged net surface heat flux (black) and precipitation minus evaporation (blue; left). Q_0 and (bottom) P-E are plotted to have roughly equivalent buoyancy flux scales.

penetrates through the base of the mixed layer depth (Q_{pen} in (1)) is estimated as $0.38 Q_{sw} \exp(-h\lambda)$, where the extinction coefficient λ^{-1} is assumed to be 20 m, consistent with Jerlov Type 1A water [Paulson and Simpson, 1977].

Figure 3 shows the daily air-sea heat flux components, as well as the net moisture flux ($P-E$). Evaporation is estimated from latent heat flux and surface temperature. Precipitation was based on the measured rain-gauge rain rate corrected for the wind distortion using the Serra *et al.* [2001] correction. The reduction in measured rain due to wind can be quite substantial. At 10 m/s the correction factor is 1.4, while at 20 m/s the correction factor is 1.83.

At KEO, where density changes are largely dominated by temperature variations, the mixed layer depth is defined as the depth where temperature is 0.2°C cooler than that at 10 m depth. At Station Papa, on the other hand, a large halocline exists near the top of the main thermocline (100–175 m depth). For this reason, for Station Papa, the mixed layer depth is defined in terms of a density step ($\Delta\sigma = 0.03 \text{ kg/m}^3$, corresponding roughly to a temperature step of 0.2°C), i.e., as the depth where density is 0.03 kg/m^3 denser than found at the 10 m level, and the isothermal surface layer thickness h_T is defined in terms of an equivalent temperature step [de Boyer Montégut *et al.*, 2004]:

$$-h = z(\sigma = \sigma|_{z=-10m} + \Delta\sigma) \quad (5a)$$

$$-h_T = z\left(T = T|_{z=-10m} + \frac{\partial T}{\partial \sigma} \Delta\sigma\right) \quad (5b)$$

If the isothermal layer is deeper than the mixed layer depth, then the layer in between, the “barrier layer,” acts as a barrier to the mixing of heat. While the mixed layer depth at KEO is well approximated by the isothermal layer depth, large barrier layers ($>15 \text{ m}$) occur at Station Papa during early spring (Figure 4). The impact of barrier layers on diffusivity calculations is discussed below.

In order to estimate the advective terms in the mixed layer heat and salt budgets, the vertically averaged mixed layer velocity (\mathbf{u}) was estimated from the moored current meter data. Both moorings generally had

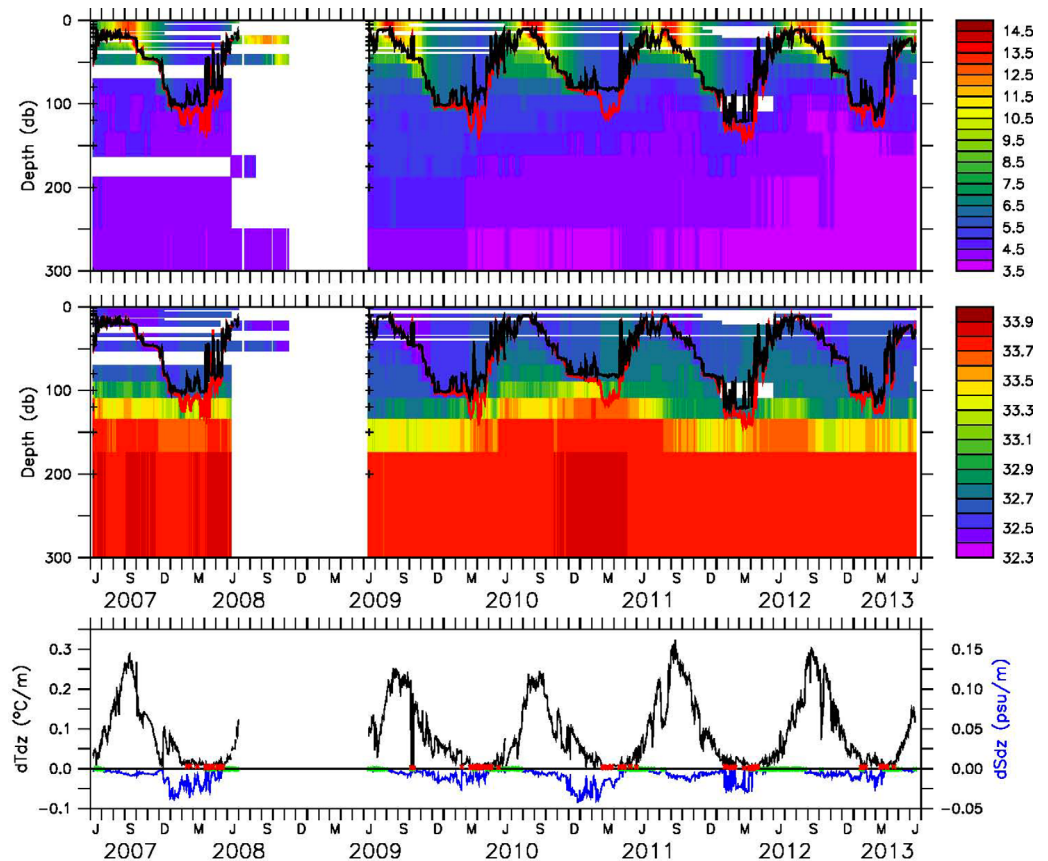


Figure 4. Daily averaged upper ocean temperature (top) and salinity (middle) time series, with mixed layer depth (black) and isothermal layer depth (red) overlaid and sensor depths indicated by plus marks at the beginning of the time series in June 2007 and June 2009. (bottom) Temperature (black) and salinity (blue) stratification in the 20 m layer below the base of the mixed layer. Weak stratification values, with an equivalent density stratification of less than 0.03 kg/m^3 over 40 m, are indicated by red and green plus mark for temperature and salinity, respectively.

up to 3 current meters mounted in the top 35 m, nominally at 5, 15, and 35 m. At KEO, data from a nearby upward looking Acoustic Doppler Current Profiler were also used to estimate \mathbf{u} during the first 2 years. When no near-surface current meter data were available, gaps in \mathbf{u} were filled with the Ocean Surface Current Analysis—Real time (OSCAR) product, which is on a $1/3$ degree grid and has 5 day resolution [Bonjean and Lagerloef, 2002]. Mixed layer temperature gradients in (1) were estimated from the Global Data Assimilation Experiment High Resolution Sea Surface Temperature (GHRSSST) 5 km product [Stark et al., 2007]. Because of the stronger currents at KEO and thus larger 1 day advective length scale there, the GHRSSST product was smoothed with a 9 point and 7 point boxcar filter at KEO and Station Papa, respectively, and then subsampled to 25 km grid before horizontal gradients were computed.

During June 2009 to January 2010 gradients in mixed layer temperature and salinity at Station Papa could also be estimated from Seaglider data [Pelland, 2015]. The glider navigated a 50 km butterfly path centered at the Station Papa mooring with a mean pattern transit time of 14.5 days. While the glider time series of mixed layer temperature agrees quite well with that of the coincident mooring and GHRSSST SST time series, the mooring and satellite data show there is significant temporal variability within this time period that aliases the glider estimate of the gradient. Mixed layer salinity, however, has less variability on this time scale and thus we use the glider estimate of the mixed layer salinity gradient to estimate advection in (2). Horizontal gradients in mixed layer-average salinity are computed at monthly intervals. Seaglider observations of S in each month are fit with a least squares regression function that is linear in x and y and quadratic in time. The monthly interval for these fields is the time required for the glider to complete two transits around the navigational track pattern at Station Papa and, as such, is approximately the shortest time scale

at which the glider array can reliably resolve horizontal gradients. The estimated x and y coefficients are taken to be the zonal and meridional components of the gradient of S during each interval. During periods when the glider was not on station and at least 4 Argo floats were present in a $300 \text{ km} \times 300 \text{ km}$ box over a given month, the Japanese Grid Point Value of the Monthly Objective Analysis using Argo data (MOAA GPV) product was used to estimate salinity gradients at Station Papa [Hosoda *et al.*, 2008]. Errors in these fields are discussed in Appendix A.

As in Cronin *et al.* [2013] (their equation (4)), vertical velocity at the base of the mixed layer was computed from the Sverdrup balance with the assumption that the turbulent stress vanishes at the base of the mixed layer. Where surface geostrophic currents are weak, such as at Station Papa, the primary term in the Sverdrup balance is the wind stress curl: $w_{-h} = (\nabla \times \tau) / (\rho f)$, where ∇ is the horizontal gradient operator, τ is the surface wind stress, ρ is density, and f is the Coriolis parameter. Daily averaged gridded QuikScat and Advanced Scatterometer (ASCAT) wind stress products made available through the Asian-Pacific Data-Research Center (<http://apdrc.soest.hawaii.edu/>) were used to estimate these terms. Similar to Cronin *et al.* [2013], the surface geostrophic current term is estimated from the AVISO Maps of Absolute Dynamic Topography (MADT) all-satellite delayed-time absolute surface geostrophic velocity gridded product (<http://www.avisos.altimetry.fr>).

With these combined mooring, satellite, glider, and float data, we are able to estimate all terms in (1) at both sites except for the term associated with diffusion of heat across the mixed layer base. That term, and in particular the eddy diffusion coefficient (i.e., diffusivity) (3a), is estimated from the residual of (1). Likewise, at Station Papa, all terms in the salt budget (2) except the diffusive salt flux term could be directly estimated for extended periods of time. The residual of (1) and (2), which we interpret in terms of diffusive mixing, however, also contains the accumulation of all errors. Thus, an error analysis (Appendix A) is performed to determine the propagation of errors in the diffusivity estimates. In order to resolve synoptic variations associated with diffusive mixing, all terms in (1) and (2) are estimated with daily averaged quantities and then smoothed with a 5-day triangular filter. The stratifications in (3) are similarly smoothed for computation of the diffusivities on synoptic time scales.

To help distinguish and remove error from the diffusivity estimate, a set of constraints is applied to the diffusivity estimate. In particular, because diffusive mixing causes a downgradient flux within a stratified fluid (3), diffusivity is only estimated if the stratification is larger than a critical level. In particular, in (3), we require temperature (or salinity) stratification to have an equivalent density stratification of 0.03 kg/m^3 over 40 m. This is somewhat arbitrary but acts to eliminate cases where the transition layer below the mixed layer is as weakly stratified as the mixed layer itself (Figure 4), periods likely dominated by error. In these cases, better vertical resolution is needed and a mixed layer depth based upon a critical stratification magnitude would be more appropriate [Brainerd and Gregg, 1995]. Because the stratification appears in the denominator in the estimation of κ , errors in stratification when it is weak can cause large errors in κ .

Likewise, following common practice, diffusivity is constrained to be positive. That is, it is assumed that diffusion results in downgradient heat and salt fluxes. Any upgradient flux value is assumed to be dominated by error and its corresponding diffusivity value (3) is not estimated. Because this constraint preferentially filters out errors of a given sign, it can bias seasonally averaged diffusivity towards larger values. At Station Papa, this constraint was applied to 11% of the data and thus is unlikely to introduce a large bias. At KEO, however, this constraint removed 37% of the data and thus could have more of an effect. Finally, when currents at KEO are strong, other processes not included in (1), such as the heat flux due to the convergence of stratified, shear flow, will be included in the residual heat flux. Thus, diffusivity is estimated at the KEO site only during periods when horizontal advection is weak (less than one standard deviation).

To further reduce errors and to provide values that could be applied more generally, monthly climatologies are computed. Indeed, sometimes only monthly climatological data are available to assess some terms (e.g., horizontal salinity gradients) in mixed layer budgets (1-2) and diffusive flux (3). Conveniently, we found that the climatological diffusivity, computed from 5 day smoothed diffusivities, was quite similar (albeit somewhat higher during winter) to the diffusivity computed from climatological stratification and heat fluxes. Such a result suggests that the climatological diffusivity shown here could be applied to climatological stratification to estimate the diffusive flux across the mixed layer according to (3).

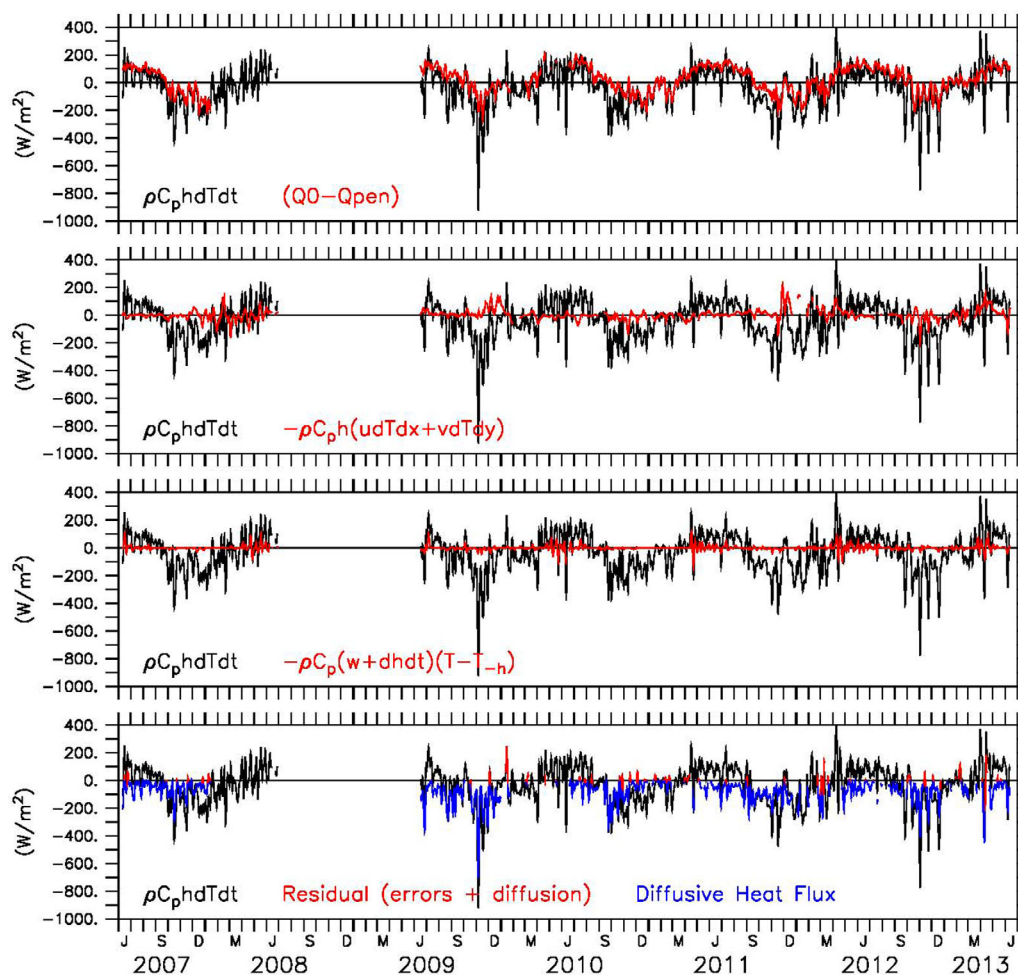


Figure 5. Station Papa mixed layer heat budget (equation (1)), smoothed with a 5 day triangular filter. The heat content tendency rate associated with changes in the mixed layer temperature (black line) is shown in all plots. The red lines represent heat fluxes in all four plots; top plot due to $Q_0 - Q_{pen}$, the second plot from top due to horizontal advection, the second plot from bottom due to entrainment, and the bottom plot due to unresolved processes and errors. The estimated diffusive flux across the base of the mixed layer is shown in blue in the bottom plot. All fluxes have units W/m^2 .

3. Results

3.1. Mixed Layer Heat and Salt Budgets at Station Papa

As shown in Figure 5, mixed layer temperature changes at Papa are strongly controlled by the surface fluxes and by the residual diffusive mixing. In particular, the net surface heat fluxes appear to control the large seasonal cycle in the surface temperature, while the residual mixing cause episodic cooling events lasting up to a few days. Cooling events associated with mixing were most prominent during summer and early fall when the mixed layer depth was still relatively shallow. Except during a few short periods, both horizontal advection and large-scale entrainment/detrainment appear to have a relatively minor effect on surface temperature.

In contrast to SST, the mixed layer salinity does not have a distinct seasonal cycle (Figures 5–7). Both evaporation and precipitation are larger during winter, with precipitation dominating (Figures 2 and 3). As a consequence, the net moisture flux into the ocean ($P - E$) at Papa tends to be positive in all seasons, with somewhat higher values during winter (Figure 7). Except for the transition periods near the equinox, the buoyancy flux is dominated by the heat flux (Figure 3), and contributes to turbulent convective mixing during winter. During winter, rather than causing surface freshening, freshwater from rainfall gets diffused into the water below the mixed layer where it strengthens the halocline (note the strong upward diffusive salt fluxes/downward freshwater fluxes during winter in Figure 6). As with the temperature balance, horizontal

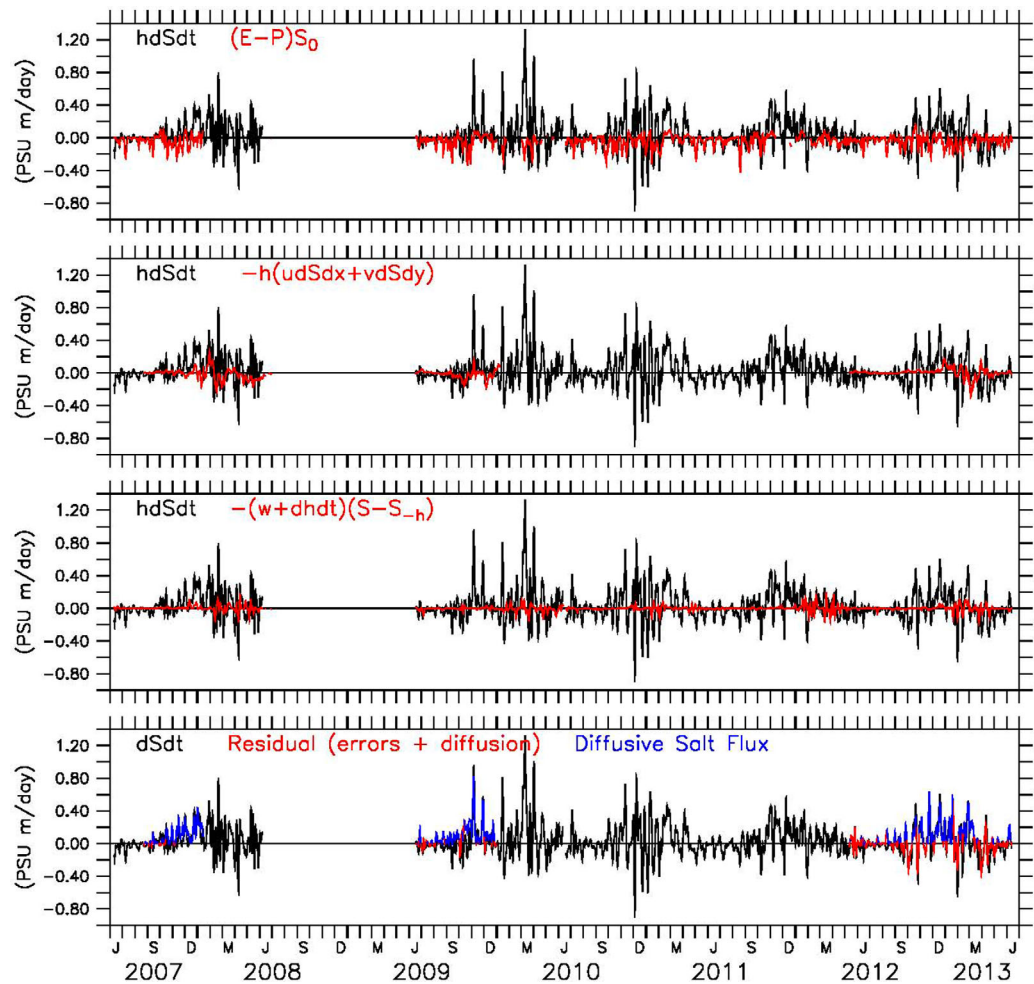


Figure 6. Same as Figure 5, but for salinity. Units are psu m/day.

salinity advection was a nonnegligible process at times. The residual diffusive mixing is nearly always positive, causing the mixed layer salinity to increase and the deeper waters to freshen.

The residual heat flux through the base of the mixed layer is relatively constant through the year, with similar values found in January–February–March as in June–July–August at Papa (Figure 7). In contrast, the salinity fluxes at the base of the mixed layer had a large seasonal cycle with large positive values during the cold season and very weak positive values during summer months. As shown in Figure 4, during late winter–early spring (particularly March and April), the mixed layer depth was deep (~100 m; Figure 4), but the isothermal layer was deeper. The layer between, the barrier layer, acts as a barrier to the mixing of heat. Due to the very weak and poorly resolved temperature stratification, diffusivity at the base of the mixed layer often cannot be estimated from the heat budget when a barrier layer is present.

Likewise, during late spring through summer as the seasonal thermocline forms, causing the mixed layer depth to shoal to less than 20 m deep, the haline stratification lies well below the base of the mixed layer and thus the diffusive flux of salt was weak. During these months, the salinity stratification is often too weak to estimate diffusivity from the salt budget (Figure 4).

3.2. Diffusivity at the Base of Mixed Layer at Station Papa

Synoptic diffusivity (κ_T and κ_S) estimated from the mixed layer heat and salt budgets for Station Papa and their associated error estimates are shown in Figure 8. In general, the errors in the diffusivity value

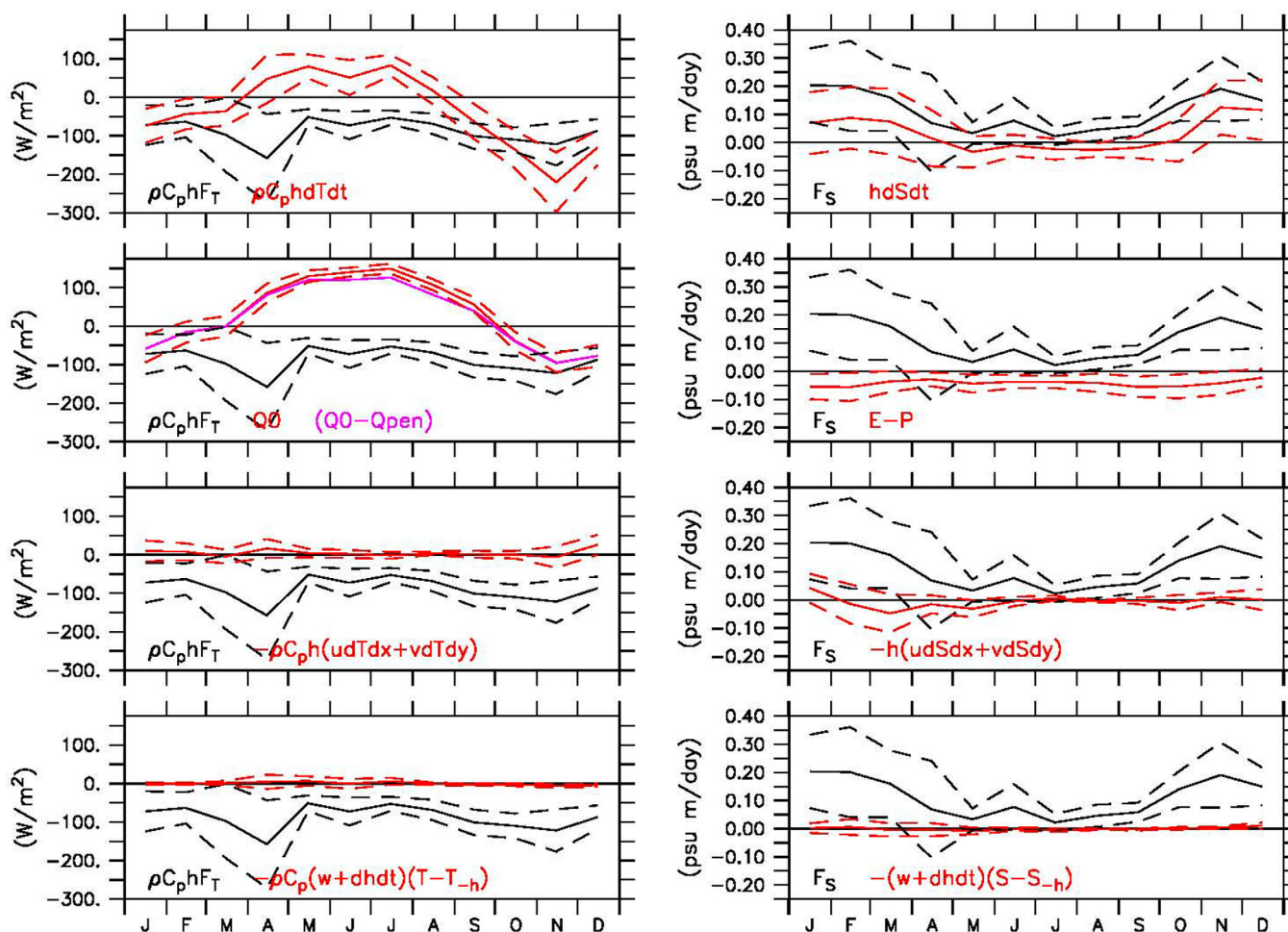


Figure 7. Monthly climatology of Station Papa heat (left) and salinity (right) budget terms shown in, respectively, Figures 5 and 6, except that the diffusive flux across the base of the mixed layer is shown in black in all plots. 68% uncertainty bounds are indicated by dashed lines.

estimated from the salt budget are larger than those estimated from the mixed layer heat budget (see Appendix A for full discussion of the errors). As shown in their scatter plot (Figure 9), the correlation coefficient for all diffusivity pairs (0.65) is significantly different than zero at the 95% confidence level for 36 degrees of freedom. Furthermore, this correlation increases to 0.83 if only June through November pairs are used, suggesting that while this appears to be a robust estimate of the mass diffusivity, the values during late winter through spring are less certain.

Diffusivity values from both budgets at Station Papa have large variability associated with the seasonal cycle and thus are best viewed on logarithmic scales, even for seasonal climatologies (Figure 10). At Papa, climatological κ_T is based upon 4–5 years of data for June–December and 1–2 years of data for winter months. For κ_S , however, only November–December has slightly more than 2 years of data, while there are no values during the month of April, one value in May, and all other months have less than a complete month each. Consequently, measurement errors are order one for climatological April κ_T and for all months except the fall for κ_S (Figure A1). Thus, even when the monthly climatologies appear to be statistically significant, caution is warranted when considering the winter values and months when the measurement errors are order one.

In summary, diffusivity associated with the diffusive heat and salt fluxes across the mixed layer base has values of $\sim 1 \times 10^{-4} m^2/s$ during the summer at Papa, increasing to $\sim 3 \times 10^{-4} m^2/s$ in November. During winter months, diffusivity appears to increase to almost $8 \times 10^{-4} m^2/s$, and possibly to even higher values during early spring, although the errors are very large during these months.

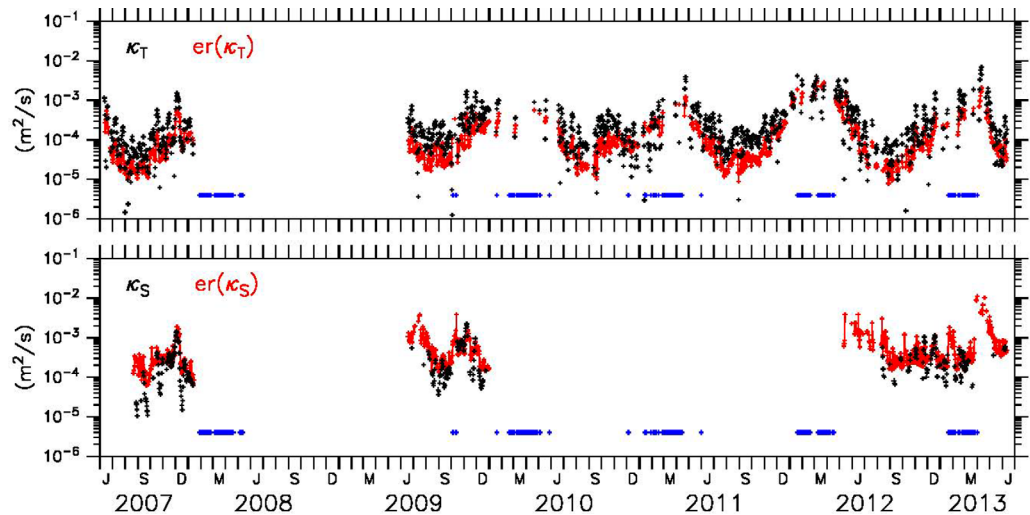


Figure 8. Time series of the diffusion coefficient (i.e., diffusivity) corresponding to the 5 day smoothed diffusive heat flux (top, black) and salinity flux (bottom, black) at the base of the mixed layer in units m^2/s . Measurement error estimate is indicate in red. Periods where the barrier layer was larger than 15 m are shown by a blue mark.

3.3. Comparison to KEO

To investigate regional variations in diffusivity and the diffusive flux across the base of the mixed layer, a corresponding analysis was performed using data from the KEO mooring. In contrast to Station Papa (Figure 5), at KEO, horizontal advection can sometimes be an order one process (Figure 11), causing the residual to be highly variable and often positive, presumably due to unaccounted advective processes. Consequently, when advection was larger than one standard deviation, the residual was not interpreted in terms of diffusive heat fluxes. Monthly climatology of each term, including estimate of the residual diffusive heat flux at the base of the mixed layer, is shown in Figure 12. It should be noted that because constraints are applied to the residual to determine the diffusive flux, the climatological diffusive flux differs from the residual (not shown), and therefore, the seasonal budgets in Figures 7 and 12 close only if the error bars are considered.

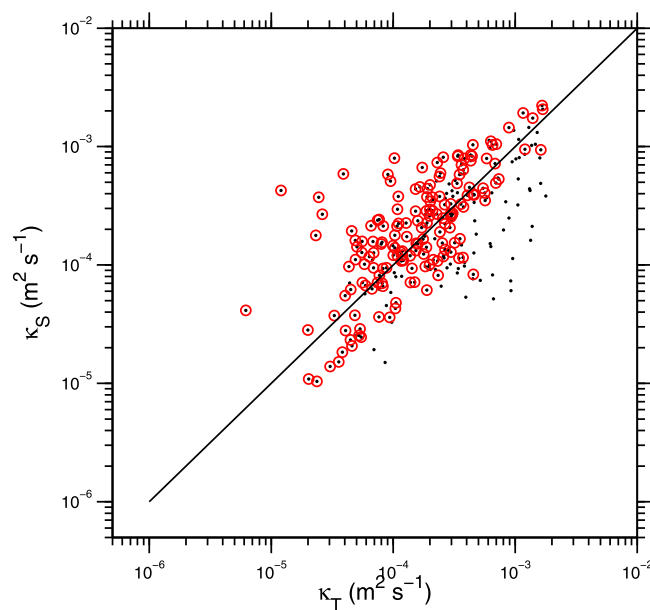


Figure 9. Scatterplot of diffusivity values estimated from the mixed layer heat and salt budgets. June–November values are indicated by red circles.

As shown in Figure 1, Station P is in a region of net surface heat gain, while KEO is in region of net surface heat loss, primarily due to wintertime values: while net surface heat loss at Station Papa reaches a climatological maximum of almost order $-100 W/m^2$ during November and December (Figure 7), at KEO, the ocean loses order $-300 W/m^2$ to the atmosphere on average during December and January (Figure 12). At both sites, the climatological synoptic diffusive flux was similar in value to these wintertime maximum surface heat loss values, although one must remember that the measurement and statistical errors are very large during these periods.

As shown in Figure 10, wintertime diffusivity values at KEO were higher than $\sim 7 \times 10^{-3} m^2/s$, at least an order of magnitude larger than the wintertime

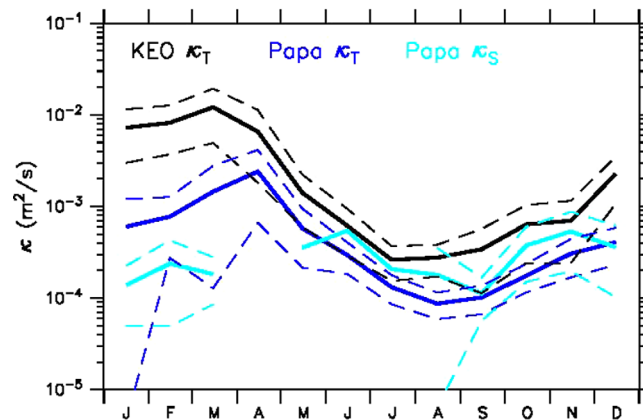


Figure 10. Monthly climatology of diffusivity at the base of the mixed layer estimated for KEO (black) and Station Papa (blue). Station Papa diffusivity estimated from the heat budget are shown in dark blue and from the salt budget are shown in light blue. 68% uncertainty bounds are indicated by dashed lines. If lower bound is not shown, the uncertainty is larger than the monthly mean value.

diffusivity values at Station Papa. During the warm season, KEO diffusivity were lower, $\sim 3 \times 10^{-4} \text{ m}^2/\text{s}$, but still more than 3 times larger than at Papa.

4. Discussion

The eddy diffusion coefficient (referred to here as diffusivity) represents the efficiency of a temporally averaged diffusive flux within a unit stratification. Thus, if the diffusivity value is known, the diffusive flux can be estimated simply from the vertical profile of the property. For many mixed layer budget estimates, and particularly for biogeochemical budgets, this is critical for any attempt at closure.

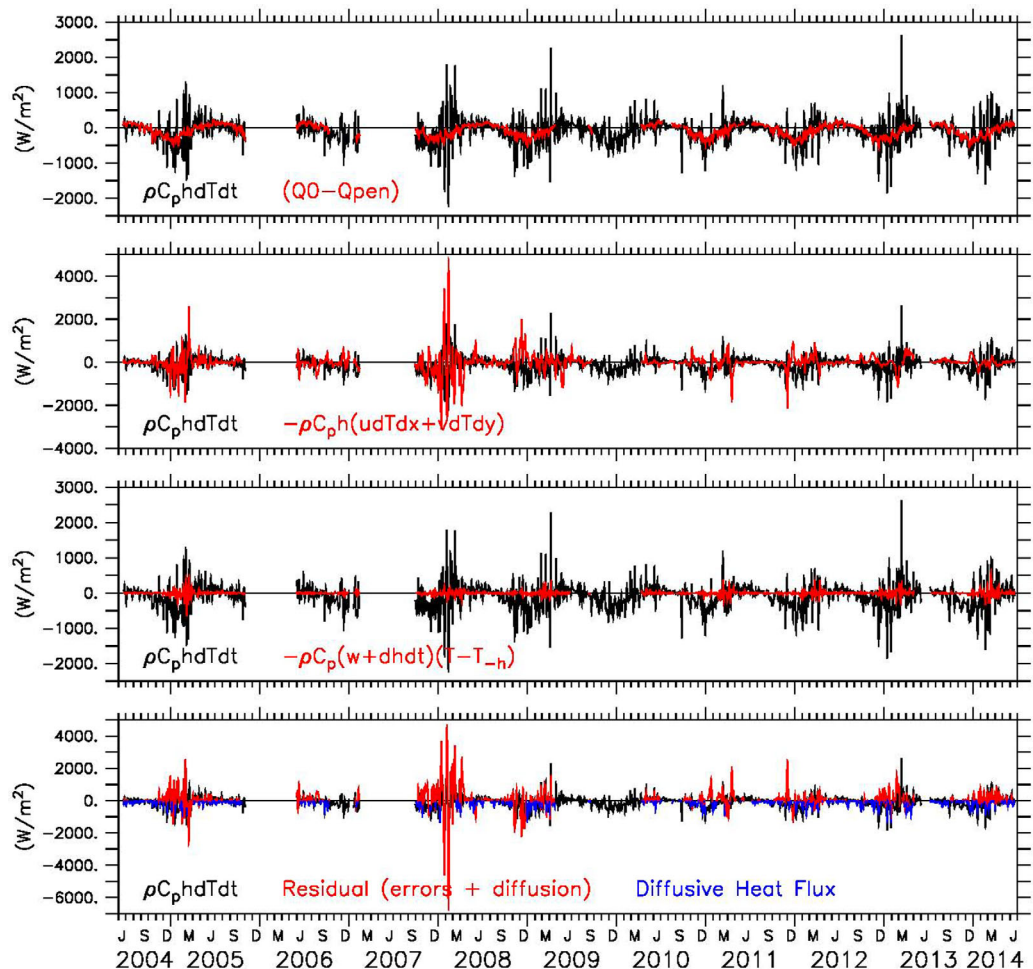


Figure 11. Same as Figure 5, but for the KEO heat budget.

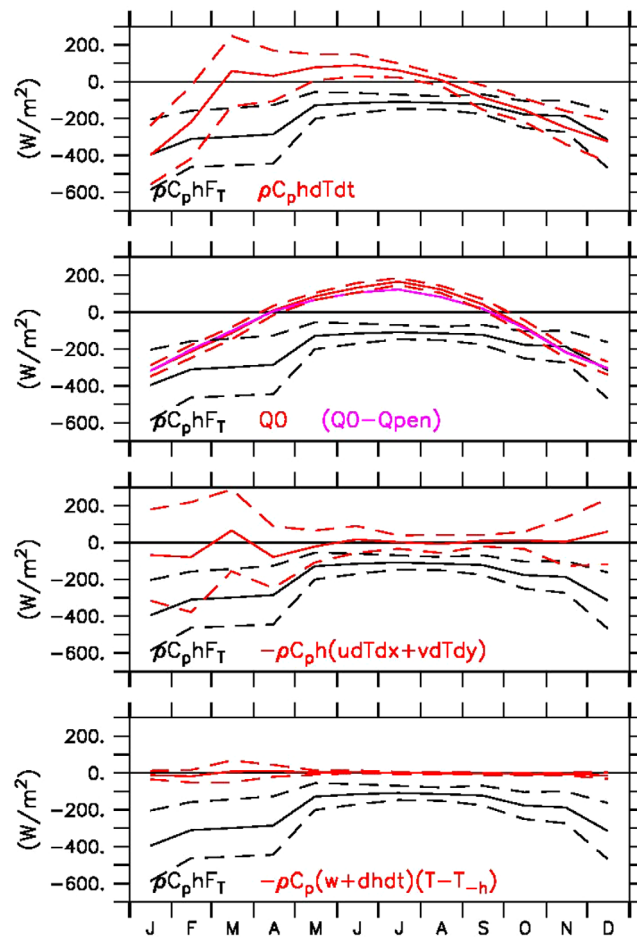


Figure 12. Same as Figure 7 left plots, but for the KEO heat budget.

In this analysis, the 5 day averaged diffusive flux at the base of the mixed layer is parameterized in terms of a diffusivity applied to the 5 day smoothed property gradient computed over the 20 m transition layer directly below the base of the mixed layer. The diffusive flux and diffusivity are estimated from the residual of the mixed layer heat and salt budgets. Several constraints are applied to filter noise from the residual diffusive flux: diffusivity was computed only when the property gradient just below the base of the mixed layer was sufficiently large to support diffusive mixing. Thus, for example, the salt budget at Station Papa could not be used during late spring through early summer when the mixed layer depth was defined entirely by the thermal stratification. Likewise, in late winter through early spring when a barrier layer often forms at Station Papa, the heat budget often could not be used to determine diffusivity. This constraint made it difficult to determine diffusivity at Papa during late winter and spring. At KEO, diffusivity was not computed when advection was strong. At both sites, negative diffusivity values were assumed to be dominated by errors and thus diffusivity was computed only

when the residual fluxes were downgradient. It should be noted that inclusion of upgradient heat fluxes when the surface loses heat to the atmosphere would tend to lower the diffusivity values during winter. However, we found (not shown) that this constraint did not qualitatively change the results at Papa and KEO, particularly when the large errors were considered. The simpler and stronger constraint (no upgradient heat fluxes) was thus used here.

All diffusivity estimates were large ($>10^{-4}$ m²/s), in agreement with recent estimates made during the heating season in the North Pacific using the Argo array and reanalysis products [Lee *et al.*, 2015]. Estimates at both locations in this study had a seasonal cycle with larger values during fall and winter, although errors were also larger in winter. At Station Papa in the subpolar gyre of the northeast Pacific, the diffusivity value was $\sim 1 \times 10^{-4}$ m²/s during summer, while during fall it increased to $\sim 3 \times 10^{-4}$ m²/s, matching the 3×10^{-4} m²/s value that Large *et al.* [1986] used to close the fall heat budget in the 1980/1981 Storm Transfer and Response Experiment. It should be noted that during individual storms, Large *et al.* [1986] showed the diffusivity at the base of the mixed layer increased to values up to 7.4×10^{-3} m²/s. Such a range is consistent with the synoptic variability in our values. During January, our Station Papa climatological diffusivity estimates appear to be as large as 6×10^{-4} m²/s, increasing to 2.4×10^{-3} m²/s by April, although the errors are order one and the diffusivity values estimated from the salt budget suggest that these values should be at maximum 2×10^{-4} m²/s. In comparison, at KEO in the northwest Pacific Ocean's Kuroshio Extension recirculation gyre, overall larger diffusivity values are found: $\sim 3 \times 10^{-4}$ m²/s during the warm season (more than 3 times larger than at Papa) and more than 7×10^{-3} m²/s during the winter.

While microstructure and dye experiments tend to show diffusivity values that are much weaker (order 10^{-5} m²/s), these generally are measured within interior of the ocean, far below the base of the mixed layer.

Indeed traditional ship-based microstructure measurements and passive tracer release observations show a several decade range in turbulence values, with a general picture of elevated rates of turbulent kinetic energy (TKE) dissipation and vertical diffusion near sources of turbulence (e.g., surface wind stress and waves, convective heat loss, bottom topography), weak dissipation and diffusivity in the interior thermocline, and rapid transitions between these two regimes over short depth intervals. For example, using microstructure measurements in the tropical and subtropical Atlantic and Pacific oceans, *Fernández-Castro et al.* [2014] compute an average diffusivity rate of $169 \times 10^{-4} \text{ m}^2/\text{s}$ in the weakly stratified mixing layer, three orders of magnitude larger than compared to the ocean interior average value of $0.59 \times 10^{-4} \text{ m}^2/\text{s}$, and an order of magnitude larger than our wintertime base of the mixed layer values at Station Papa. Similarly, *Lozovatsky et al.* [2006] find diffusivities of 10^{-2} – $10^{-1} \text{ m}^2/\text{s}$ in the mixed layer and 10^{-5} – $10^{-4} \text{ m}^2/\text{s}$ in the pycnocline, separated by a 20–30 m thick transition layer over which diffusivity changes rapidly in the vertical. Likewise, *Sun et al.* [2013] show dissipation rates of TKE in the near-surface transition layer that are 5–10 times larger than those found in the upper thermocline. Our analysis focuses on turbulent exchange at the base of the surface mixed layer, in the upper portion of this near-surface stratified transition layer.

Our study suggests enhanced diffusivity in western boundary current regions, with values at least 3–4 times larger at KEO than observed at Station Papa. Enhanced turbulent mixing and diffusivity values in the thermocline near KEO were also observed by *Jing and Wu* [2014] using profiler measurements collected during the Kuroshio Extension System Study (KESS). *Jing and Wu* [2014] suggest that vorticity associated with cyclonic eddies in this region cause near-inertial energy to penetrate deep into the ocean. To explain enhanced diffusivity at the base of the mixed layer estimated from the potential vorticity budget, *Qiu et al.* [2006] hypothesize that the presence of weakly stratified Sub-Tropical Mode Water (STMW) below the seasonal thermocline acts as a barrier to internal wave energy and turbulent mixing, enhancing the turbulent mixing and diffusivity within and above the seasonal thermocline in the region south of the Kuroshio Extension. *Tomita et al.* [2010] show that typhoons are ubiquitous in the KEO region during the warm season. As these storms transition to midlatitude storms, the wind patterns become asymmetric making them much more effective at generating near inertial oscillations (NIO) throughout a broad region [*Bond et al.*, 2011]. Consequently, in contrast to Station Papa where NIO occur almost exclusively during fall and winter [*Alford et al.*, 2012], at KEO, NIO are observed year-round [*Cronin et al.*, 2013]. The higher diffusivity values found at KEO during the warm season are thus likely related to several factors, including stratification, eddies, and the strong forcing from transitioning tropical cyclones.

Because the KEO and Papa wind forcing are likely more similar during winter, the larger wintertime diffusivity values at KEO are most likely related to stratification differences there. Wintertime mixed layer depth can be very deep when STMW ventilates in the Kuroshio Extension region, allowing deep convective cells that can increase turbulent mixing at the base of the mixed layer. The influence of boundary layer depth variations and surface forced convective cells on diffusivity is a key feature of the *Large et al.* [1994] parameterization and may play a role in the different wintertime values between the two sites considered here. Using KEO and KESS data, *Cronin et al.* [2013] showed that during wintertime, the Richardson number at the base of the mixed layer was often below the critical value of 0.25 for shear instability to occur. It was hypothesized that during periods of STMW ventilation, the stratification just below the base of the mixed layer is very weak, thus making conditions favorable for shear instability. Deep convective cells, however, could also be a factor in reducing the stratification and increasing the turbulent mixing. In contrast, at Station Papa in the subpolar gyre of the northeast Pacific, the main pycnocline is relatively shallow and enhanced by a shallow halocline. Thus, while winter storms can generate significant NIO [*Alford et al.*, 2012] and turbulence, they are less efficient at generating a diffusive flux across a unit stratification.

This study provides evidence for strong seasonal and geographic patterns in the diffusivity corresponding to the diffusive flux at the base of the surface mixed layer. These temporal and spatial variations are likely related to large-scale variations in surface wind stress, buoyancy forcing, boundary layer depth, near-inertial shear, and stratification within the transition layer, as well as to the influence of surface waves, eddies, and currents. Given the importance of vertical transport at the mixed layer base to the cycling of physical and biogeochemical oceanic tracers, the relative influence of these effects on turbulent mixing there warrant further research.

Table 1. Sources of Errors in Daily Averaged Quantities^a

Source of Error	Error Value	Rank for κ_T	Rank for κ_S
Surface turbulent heat flux	Random: $4 \text{ W/m}^2 + 2\%$ Bias: -5.7 W/m^2	4	*
Radiative heat fluxes	Bias: 1%		
Evaporation	$\text{er}(Q_{\text{lat}})/(L\rho)$, where Q_{lat} is the latent heat flux, L is latent heat of evaporation and ρ is density of rainwater.	*	6
Precipitation	Random: 10%, bias: 10%	*	5
Mixed layer depth	Bias: (vertical spacing of temperature sensors spanning h)/4	2	1
Seabird temperature and salinity sensors	Bias: 0.004°C , 0.02 psu	5	2
Current meter and ADCP velocity errors	Bias: 0.01 m/s	1	4
Current errors and extrapolation within mixed layer below 15m	Bias: $1.5 \times 10^{-3} \text{ s}^{-1} \times \text{depth}$, or 0.01 ms^{-1} whichever is largest		
Vertical velocity	Random: 30%	6	7
Horizontal ∇T	Bias: $1 \times 10^{-6} \text{ }^\circ\text{C/m}$	3	*
Horizontal ∇S	Bias: Glider: $0.5\text{--}1.8 \times 10^{-7} \text{ psu/m}$; Bias: Argo: $2.8 \times 10^{-7} \text{ psu/m}$	*	3

^aErrors due to horizontal current extrapolation, horizontal temperature gradient, and vertical velocity are assumed to be biases over a 5 day time scale. Except where indicated as random errors, all errors are assumed to be biases for the entirety of the 1 year deployment. The errors are ranked in terms of their mean value for Papa. A rank of 1 indicates this is the largest source of error in the diffusivity estimate. An asterisk indicates that this quantity does not enter the calculation.

5. Conclusions

While the diffusivity values estimated from mixed layer heat and salt budgets at Station Papa had large discrepancies during winter when their errors were large, the summer and fall values agreed reasonably well, suggesting that these values may be applied to other budgets. For example, Fassbender et al. (submitted manuscript, 2015) shows that the diffusive flux of dissolved inorganic carbon across the base of the mixed layer, estimated with the diffusivity values calculated here, play an order one role in the carbon cycle of the North Pacific. Indeed, with this information, biological processes affecting the carbon cycle can be inferred, such as carbon export associated with net community production and calcification.

Appendix A: Error Analysis

Measurement errors of the 5 day mean values are estimated through propagation of errors following Cronin et al. [2013] (see their Appendix A for daily averaged values), taking into consideration random and bias errors (Table 1). Errors that are random are reduced by the square root of the degrees of freedom, where

there could be up to 4.4 degrees of freedom per month for each of the years included in the climatology. Errors that are considered biases (e.g., associated with unknown calibration offsets) are assumed to have only one degree of freedom for each year included in the climatology.

Errors in vertical velocity are increased in this analysis to 30%, although this is somewhat arbitrary. Precipitation, corrected for wind distortion, was assumed to have an unknown bias of 10% and a random error of 10% [Serra et al., 2001]. For the glider estimate of the monthly salinity gradient, errors are estimated by evaluating the sensitivity of the least-squares regression fit to the addition of random noise. In

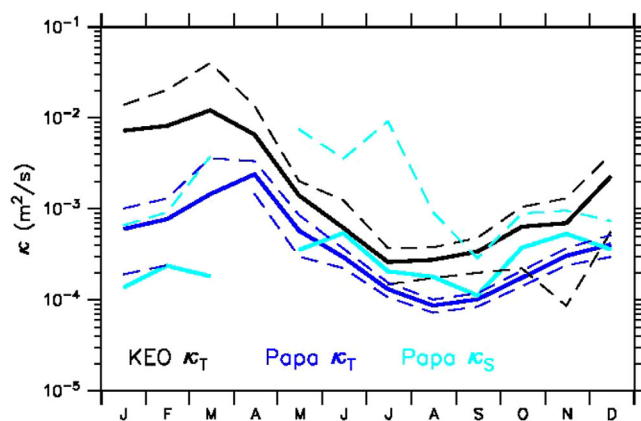


Figure A1. Monthly climatology of diffusivity at the base of the mixed layer estimated from KEO (black) and Station Papa (blue). Station Papa diffusivity estimated from the heat budget is shown in dark blue and from the salt budget is shown in light blue. Standard measurement errors are indicated by dashed lines. If lower bound is not shown, the measurement error is larger than the monthly mean value.

particular, for each month, 100 iterations of the noise-perturbed regression fits were performed. For each, the variance and time correlation of the noise was prescribed to be similar to the residuals between the data from the original estimated fit. The 68% uncertainty for each month was then computed as the standard deviation of the noise-perturbed x - and y -gradients across 100 iterations of this procedure. When glider data are unavailable, but at least four Argo floats in a 300 km \times 300 km box centered at Station Papa are available, surface salinity gradients are computed from 10 m level Argo MOAA GPV product. With four floats included in the mapping procedure, it was assumed the gridded values had a 15% variance error. The gradients, computed over a 150 km scale, thus produce a salinity gradient error in each component of 2.8×10^{-7} psu/m. All other errors listed were discussed in Cronin *et al.* [2013]. Figure A1 shows the climatological diffusivity values for KEO and Papa with their associated measurement errors.

Acknowledgments

This work was funded by the NOAA Office of Climate Observations. Station Papa shiptime has been provided by the DFO Line P program. Shiptime for KEO was provided by NSF for 2004–2006, and thereafter through a partnership between NOAA and JAMSTEC. We thank Marie Robert of the Line P program, and the captains, crews, and science parties for their help in making this study possible. Data from the NOAA surface moorings used in this study can be accessed from <http://www.pmel.noaa.gov/OCS/>. This is PMEL contribution 4167.

References

- Alford, M. H., M. F. Cronin, and J. M. Klymak (2012), Annual cycle and depth penetration of wind-generated near-inertial internal waves at Ocean Station Papa in the northeast Pacific, *J. Phys. Oceanogr.*, *42*(6), 889–909.
- Bond, N. A., M. F. Cronin, C. Sabine, Y. Kawai, H. Ichikawa, P. Freitag, and K. Ronnholm (2011), Upper-ocean response to typhoon Choi-Wan as measured by the Kuroshio Extension Observatory (KEO) mooring, *J. Geophys. Res.*, *116*, C02031, doi:10.1029/2010JC006548.
- Bonjean, F., and G. S. E. Lagerloef (2002), Diagnostic model and analysis of the surface currents in the tropical Pacific Ocean, *J. Phys. Oceanogr.*, *32*, 2938–2954.
- Brainerd, K. E., and M. C. Gregg (1995), Surface mixed and mixing layer depths, *Deep Sea Res., Part I*, *42*, 1521–1543.
- Cronin, M. F., N. A. Bond, J. T. Farrar, H. Ichikawa, S. R. Jayne, Y. Kawai, M. Konda, B. Qiu, L. Rainville, and H. Tomita (2013), Formation and erosion of the seasonal thermocline in the Kuroshio Extension recirculation gyre, *Deep Sea Res., Part II*, *85*, 62–74, doi:10.1016/j.dsr2.2012.07.018.
- de Boyer Montégut, C., G. Madec, A. S. Fischer, A. Lazar, and D. Iudicone (2004), Mixed layer depth over the global ocean: An examination of profile data and a profile-based climatology, *J. Geophys. Res.*, *109*, C12003, doi:10.1029/2004JC002378.
- Dohan, K., and R. E. Davis (2011), Mixing in the transition layer during two storm events, *J. Phys. Oceanogr.*, *41*, 42–66, doi:10.1175/2010JPO4253.1.
- Emerson, S., and C. Stump (2010), Net biological oxygen production in the ocean: II. Remote in situ measurements of O₂ and N₂ in subarctic Pacific surface waters, *Deep Sea Res., Part I*, *57*(10), 1255–1265, doi:10.1016/j.dsr.2010.06.001.
- Emerson, S., C. Sabine, M. F. Cronin, R. Feely, S. E. Cullison Gray, and M. DeGrandpre (2011), Quantifying the flux of CaCO₃ and organic carbon from the surface ocean using in situ measurements of O₂, N₂, pCO₂, and pH, *Global Biogeochem. Cycles*, *25*, GB3008, doi:10.1029/2010GB003924.
- Fairall, C. F., E. F. Bradley, J. E. Hare, A. A. Grachev, and J. B. Edson (2003), Bulk parameterization of air-sea fluxes: Updates and verification for the COARE algorithm, *J. Clim.*, *16*, 571–591, doi:10.1175/1520-0442(2003)016<0571:BPOASF>2.0.CO;2.
- Fernández-Castro, B., B. Mouriño-Carballido, V. M. Benítez-Barrios, P. Chouciño, E. Fraile-Nuez, R. Graña, M. Piedeleu, and A. Rodríguez-Santana (2014), Microstructure turbulence and diffusivity parameterization in the tropical and subtropical Atlantic, Pacific and Indian Oceans during the Malaspina 2010 expedition, *Deep Sea Res., Part I*, *94*, 15–30.
- Hosoda, S., T. Ohira, and T. Nakamura (2008), A monthly mean dataset of global oceanic temperature and salinity derived from Argo float observations, *JAMSTEC Rep. Res. Dev.*, *8*, 47–59.
- Jing, Z., and L. Wu (2014), Intensified diapycnal mixing in the midlatitude western boundary currents, *Sci. Rep.*, *4*, 7412, doi:10.1038/srep07412.
- Kubota, M., N. Iwabe, M. F. Cronin, and H. Tomita (2008), Surface heat fluxes from the NCEP/NCAR and NCEP/DOE reanalyses at the KEO buoy site, *J. Geophys. Res.*, *113*, C02009, doi:10.1020/2007JC004338.
- Large, W. G., and G. B. Crawford (1995), Observations and simulations of upper-ocean response to wind events during the Ocean Storms Experiment, *J. Phys. Oceanogr.*, *25*, 2831–2852.
- Large, W. G., J. C. McWilliams, and P. P. Niiler (1986), Upper ocean thermal response to strong autumnal forcing of the northeast Pacific, *J. Phys. Oceanogr.*, *16*, 1524–1550.
- Large, W. G., J. C. McWilliams, and S. C. Doney (1994), Oceanic vertical mixing: A review and a model with a nonlocal boundary layer parameterization, *Rev. Geophys.*, *32*, 363–403.
- Ledwell, J. R., L. C. St. Laurent, J. B. Girton, and J. M. Toole (2011), Diapycnal mixing in the Antarctic Circumpolar Current, *J. Phys. Oceanogr.*, *41*, 241–246, doi:10.1175/2010JPO4557.1.
- Lee, E., Y. Noh, B. Qiu, and S.-W. Yeh (2015), Seasonal variation of the upper ocean responding to surface heating in the North Pacific, *J. Geophys. Res. Oceans*, *120*, 5631–5647, doi:10.1002/2015JC010800.
- Lozovatsky, I., E. Roget, H. Fernando, M. Figueroa, and S. Shapovalov (2006), Sheared turbulence in a weakly stratified upper ocean, *Deep Sea Res., Part I*, *53*(2), 387–407, doi:10.1175/2010JPO4557.1.
- Niiler, P. P., N. A. Maximenko, and J. C. McWilliams (2003), Dynamically balanced absolute sea level of the global ocean derived from near-surface velocity observations, *Geophys. Res. Lett.*, *30*, 2164, doi:10.1029/2003GL018628.
- Paulson, C. A., and J. J. Simpson (1977), Irradiance measurements in the upper ocean, *J. Phys. Oceanogr.*, *77*, 952–956, doi:10.1175/1520-0485(1977)007<0952:IMITUO>2.0.CO;2.
- Pelland, N. A. (2015), Eddy circulation, heat and salt balances, and ocean metabolism: Observations from a Seaglider-Mooring array at Ocean Station Papa, Ph.D. thesis, Univ. of Wash, ProQuest/UMI. Ann Arbor, Mich.
- Polzin, K. L., J. M. Toole, J. R. Ledwell, and R. W. Schmitt (1997), Spatial variability of turbulent mixing in the abyssal ocean, *Science*, *276*(5309), 93–96.
- Qiu, B., P. Hacker, S. Chen, K. A. Donohue, D. R. Watts, H. Mitsudera, N. G. Hogg, and S. R. Jayne (2006), Observations of the Subtropical Mode Water evolution from the Kuroshio Extension System Study, *J. Phys. Oceanogr.*, *36*, 457–473.
- Schmitt, R. W., J. M. Toole, R. L. Koehler, E. C. Mellinger, and K. W. Doherty (1988), The development of a fine- and microstructure profiler, *J. Atmos. Oceanic Technol.*, *5*, 484–500.
- Send, U., et al. (2010), OceanSITES, in *Proceedings of the "OceanObs'09: Sustained Ocean Observations and Information for Society" Conference, vol. 2, Venice, Italy, September 2009*, edited by J. Hall et al., ESA Publ. WPP-306, doi:10.5270/OceanObs09.cwp.79.

- Serra, Y. L., P. A'Hearn, H. P. Freitag, and M. J. McPhaden (2001), ATLAS self-siphoning rain gauge error estimates*, *J. Atmos. Oceanic Technol.*, *18*, 1989–2002, doi:10.1175/1520-0426(2001)018 <1989:ASSRGE>2.0.CO;2.
- Stark, J. D., C. J. Donlon, M. J. Martin, and M. E. McCulloch (2007), OSTIA: An operational, high resolution, real time, global sea surface temperature analysis system, paper presented at Oceans 2007: Marine Challenges: Coastline to Deep Sea, IEEE/Oceanic Eng. Soc., Aberdeen, Scotland, 18–21 June.
- Stevenson, J. W., and P. P. Niiler (1983), Upper ocean heat budget during the Hawaii-to-Tahiti shuttle experiment, *J. Phys. Oceanogr.*, *13*, 1894–1907, doi:10.1175/1520-0485(1983)013 <1894:UOHBDT>2.0.CO;2.
- Sun, O. M., S. R. Jayne, K. L. Polzin, B. A. Rahter, and L. C. St. Laurent (2013), Scaling turbulent dissipation in the transition layer, *J. Phys. Oceanogr.*, *43*, 2475–2489, doi:10.1175/JPO-D-13-057.1.
- Tomita, H., S. Kako, M. F. Cronin, and M. Kubota (2010), Preconditioning of the wintertime mixed layer at the Kuroshio Extension Observatory, *J. Geophys. Res.*, *115*, C12053, doi:10.1029/2010JC006373.